Piezoresistive response of epoxy composites with carbon nanoparticles under tensile load

Malte H. G. Wichmann,* Samuel T. Buschhorn, Jan Gehrmann, and Karl Schulte
Institute of Polymers and Composites, Technische Universität Hamburg–Harburg, Denickestrasse 15, 21073 Hamburg, Germany
(Received 23 April 2009; revised manuscript received 7 October 2009; published 29 December 2009)

In this paper, electrically conductive epoxy based nanocomposites based on multiwall carbon nanotubes and carbon black were investigated concerning their potential for strain sensing applications with electrical conductivity methods. This paper aims to investigate the electromechanical response of the nanocomposite matrices subjected to mechanical load. It was found that the nanocomposites exhibit a distinct resistance vs strain behavior in the regime of elastic deformation, which is in good agreement with prevalent theories about charge carrier transport mechanisms in isolator/conductor composites. Applying an analytical model, it could be shown that the piezoresistivity of nanocomposites may contribute valuable information about the conductive network structure and charge carrier transport mechanisms occurring in the nanocomposites.

DOI: 10.1103/PhysRevB.80.245437 PACS number(s): 73.63.Fg, 72.80.Tm, 72.20.Fr, 72.60.+g

I. INTRODUCTION

One of the main disadvantages of composite structures is that inspection and assessment of the mechanical condition is challenging. Composite parts are highly heterogeneous and nontransparent, thus a nondestructive investigation (NDI) or *in situ* health monitoring of composite parts under dynamic loading conditions is difficult to perform. In recent years, health monitoring technologies have therefore attracted great interest in composites science, especially motivated by the developments in the aircraft industry, where composite parts are critical for operational safety. Another important development is the trend toward off-shore wind energy parks, where inspection and maintenance could be significantly supported by these techniques. The most important benefits of a real-time, *in situ* health monitoring would be an increase in safety by the prevention of catastrophic failures and the reduction of maintenance costs, by optimizing inspection cycles. In the optimum case, a health monitoring system could provide a quick assessment of damage location and damage extent. Typical damage in composites structures are interfacial and interlaminar cracking, fiber breakage, surface cracks, delaminations, propagating fatigue cracks, and corrosion. Especially intrinsic damage, such as matrix cracking and delamination are very difficult to detect with conventional NDI methods.

The potential of electrically conductive nanocomposite matrix systems for sensing damage, as well as stresses/strains in fiber reinforced composite materials has been proven in various experimental setups.[1–5] It could be shown that thermosetting matrix systems loaded with very small volume contents ($\Phi < 1$ vol %) of conductive nanoparticles, such as carbon black (CB) and multiwall carbon nanotubes (MWCNTs), exhibit distinct piezoresistive properties, enabling the electrical measurement of apparent mechanical load on the composite specimen.

The piezoresistive response of particle modified polymers has been extensively analyzed in the past. The first systems investigated in this context were highly filled carbon black rubber systems.[6–11] These studies have shown that the electrical resistance behavior of the carbon black/rubber composite can deliver valuable information on the network structure and reinforcing mechanisms of the carbon black.

The first comprehensive study on the piezoresistive properties of carbon/epoxy composites was conducted by Carmona *et al.*[12] They investigated the influence of hydrostatic pressure on the resistivity of CB/epoxy and short carbon fiber (SCF)/epoxy composites. The reason for the piezoresistive behavior was clearly connected to the heterogeneous structure of the composite, as the authors emphasize that the constituents of the composites do not necessarily need to exhibit intrinsic piezoresistive properties. A similar study by Wang *et al.*[13] yielded comparable results. Further experimental studies conducted on different systems, e.g., polypropylene/graphite,[14] epoxy/graphite,[15] and PE, PS and epoxy based metal particle composites[16] all deliver the same qualitative results, revealing a distinct piezoresistive behavior.

The application of conductive nanoparticles for the manufacturing of conductive nanocomposites has been extensively studied in the past decade. Conductive carbon nanoparticles such as carbon black, carbon nanofibers, and carbon nanotubes are suitable candidates for the production of conductive nanocomposites, utilizing only very low volume contents ($\Phi < 1$ vol %). In their study on soft thermoplastic matrices, Flandin *et al.*, first explicitly applied conductive nanoparticles to investigate the potential of these materials as sensors for mechanical strain and damage.[17,18] They found that the nanoparticles provide a very smooth and noise free piezoresistive effect. Knite *et al.* were able to correlate the piezoresistive behavior of a nanoscaled carbon black/polyisoprene composite[19,20] to the change in interparticle distances. Studies on the piezoresistive effect in carbon nanotube based composites revealed comparable results.[21–29] The macroscopic electrical behavior and the piezoresistive response in the elastic regime are usually found to be well explained by the tunneling theory of Simmons,[30–33] later extended by Sheng *et al.*,[34–37] who considered the influence of temperature on the electrical properties of an isolator/conductor composite. These models predict an exponential increase of the interparticle tunneling resistances with increasing particle separation. The often cited relationship between electrical conductivity σ and the particle volume content Φ in particle reinforced composites of $\ln \sigma \sim \Phi^{-1/3}$ is

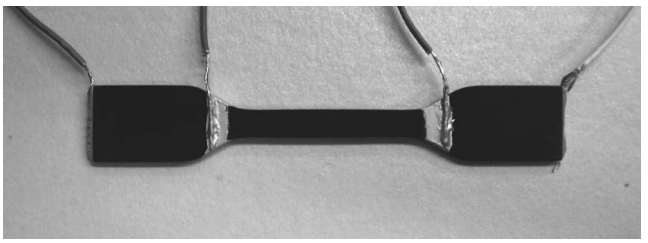

FIG. 1. A contacted tensile test specimen with four contacts. The current was injected at the outer contacts, while the voltage was measured at the inner electrodes during the tensile tests.

derived from these models,[38] assuming a statistical distribution of the particles in the isolating matrix.

In this work, the piezoresistive responses of carbon black and carbon nanotube/epoxy composite systems with very low filler contents are analyzed in detail. The electrical resistance behavior under tensile load is analyzed in the elastic as well as in the inelastic regime. The influence of particle volume fraction and particle geometry on the macroscopic electrical response is investigated. Furthermore, the piezoresistive response in the elastic regime is correlated with existing analytical models. It is demonstrated that the macroscopic resistance behavior of conductive nanocomposites subjected to mechanical load may contribute valuable information about the intrinsic particle network structure and the apparent conduction mechanisms.

II. EXPERIMENTAL

Epoxy nanocomposites with different volume contents of multiwall carbon nanotube and carbon black were produced via a high shear mixing process involving a three roller mill.[40] As matrix system, the Araldite LY556 epoxy system, the Aradur 917 anhydride hardener and the D070 accelerator, provided by Huntsman, Switzerland, was used. CVD-grown MWCNTs, provided by Arkema, France, as well as carbon black XE2, provided by Evonik Degussa, Germany, were applied. Filler contents of 0.1 and 0.3 wt. % for the MWCNT nanocomposites and 0.5 wt. % for the carbon black nanocomposite were chosen. This was done to tune the electrical conductivity over a range of two orders of magnitudes and to investigate a possible influence of filler content on the sensitivity of the nanocomposite sensors. The carbon black nanocomposite was investigated for comparative reasons, as the primary particles are of a spherical nature and exhibit an aspect ratio of around one (compared to several hundred for MWCNTs).

The tensile tests were performed using a Zwick Z010 universal testing machine, according to DIN EN ISO 527.1. A crosshead speed of 1 mm/min was applied. Dog-bone specimens were prepared according to DIN EN ISO 527.2 by countersinking. The elongation of the specimens was measured optically, using a laser extensometer. For the electrical resistance measurements, the samples were contacted at the ends and at the ends of the parallel part with a surface-ring contact of conductive silver paint in order to allow for a four-probe measurement. A photograph of a contacted specimen is given in Fig. 1. A Keithley Sourcemeter 2602 was used for resistance measurements, performed simultaneously to the mechanical tests. For each sample, the current was chosen to produce an initial potential of $U=10$ V between the measurement electrodes. At least seven specimens were tested for each material produced.

TABLE I. Average ac conductivity values and standard deviations.

Material	σ (S/m)
0.1 wt. % MWCNTs	$2.0\times10^{-4}\pm1.27\times10^{-4}$
0.3 wt. % MWCNTs	$1.32\times10^{-2}\pm2.06\times10^{-3}$
0.5 wt. % CB	$2.49\times10^{-3}\pm1.67\times10^{-4}$

III. RESULTS AND DISCUSSION

A. Nanocomposite characterization

The conductivities of the nanocomposites produced are given in Table I. The 0.1 wt. % MWCNT nanocomposite exhibited a conductivity of about 2×10^{-4} S/m; the 0.3 wt. % MWCNT nanocomposite showed a value of about 1.3×10^{-2} S/m. For the carbon black nanocomposite, a conductivity of about 2.5×10^{-3} S/m was measured. The conductivity values for the 0.1 and 0.3 wt. % nanocomposite differ by two orders of magnitude. The filler content of 0.5 wt. % for carbon black was chosen as it yields a conductivity value in between the two carbon nanotube composites. It is one order of magnitude higher than the conductivity of the 0.1 wt. % MWCNT composite and one order of magnitude lower than the 0.3 wt. % MWCNT nanocomposite. Figure 2 shows the electrical conductivity vs electric field behavior of the nanocomposites investigated. As the charge carrier transport in such composites is dominated by the interparticle contacts, they generally behave non-Ohmic. The non-Ohmic behavior is known to become more significant

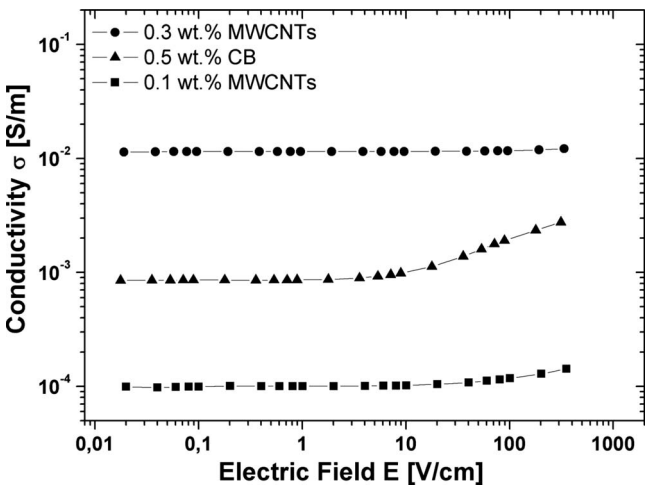

FIG. 2. Electrical conductivity vs field strength of the three different nanocomposites.

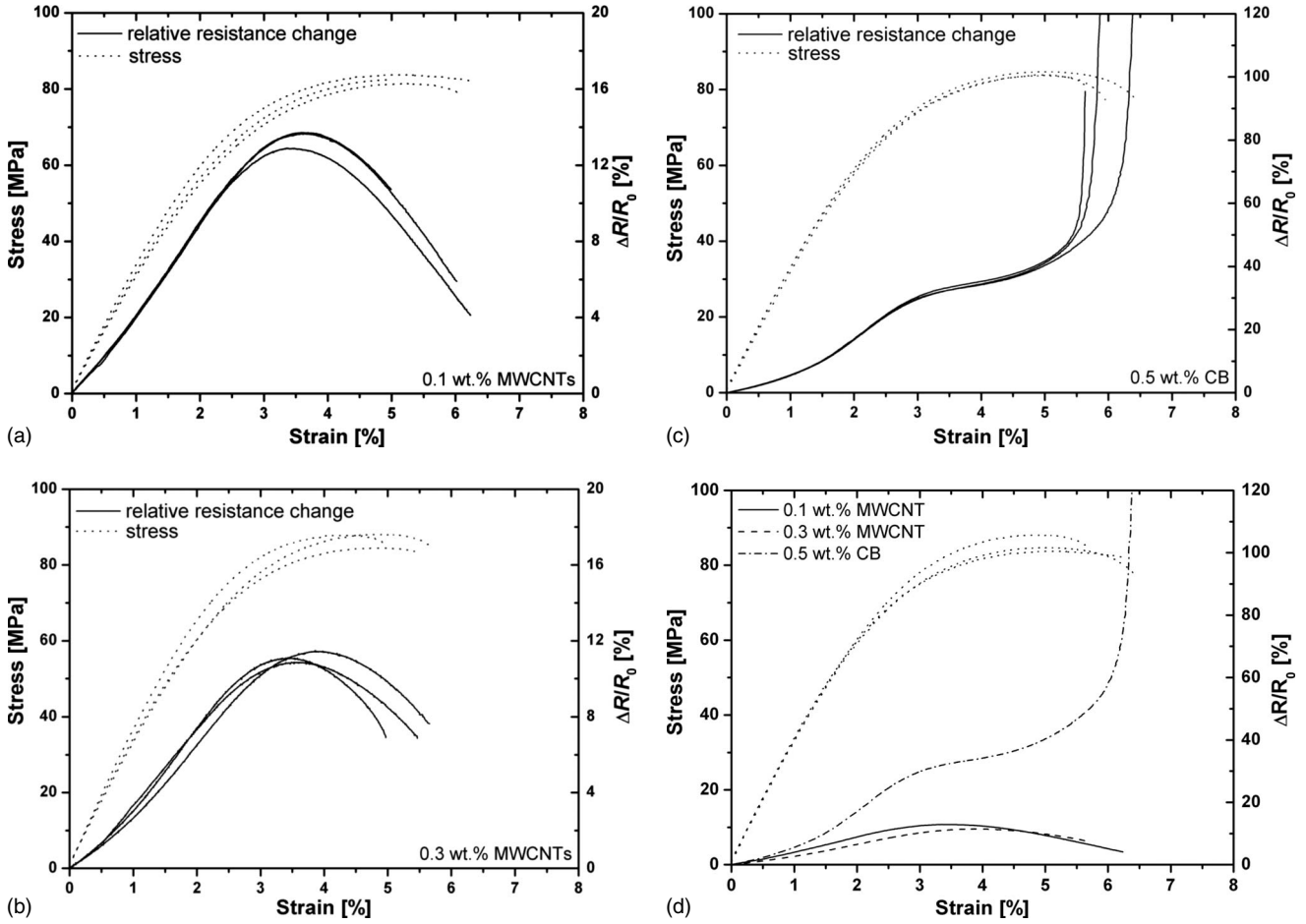

FIG. 3. Electrical resistance change vs tensile strain for (a) the 0.1 wt. % MWCNT composite, (b) the 0.3 wt. % MWCNT composite, (c) the 0.5 wt. % CB composite. Representative curves of the different composites are combined in (d) for comparative purposes. The mechanical stress/strain curves are shown as dotted lines in all diagrams.

close to the percolation threshold.[39] From Fig. 2, it can be seen that the nanocomposites investigated in this study show a quasi-Ohmic behavior at low electrical field strength values and a weak deviation from Ohmic behavior occurs at higher values. The electric field strength applied during the tensile tests was around 4 V/cm, ranging within the regime of quasi-Ohmic behavior.

It should be noted that in both types of nanocomposites, the electrically conductive network is formed by kinetic percolation during the curing process,[40,41] as is typically observed for carbon nanoparticle/epoxy composites. A recent synopsis on this issue can be found in Ref. 42. This implies that the average interparticle distances cannot be simply calculated from the particle volume content. Indeed, a quantitative description of conducting network structures is difficult to perform and matter of many ongoing studies, mostly involving numerical modeling.[43–46] The analysis of the piezoresistive response may contribute significantly to the characterization of these network structures, as shown in the following chapters.

B. Tensile tests

Exemplary results of the tensile tests are shown in Figs. 3(a)–3(c). Mechanical stress/strain curves are shown as dotted lines. The nanocomposites exhibit strain to failure values between 6–7 % and tensile strength values between 85–90 MPa, being in excellent agreement with the manufacturers' data for the epoxy matrix system LY556/Aradur 917/D070. The solid curves in Figs. 3(a)–3(c) represent the corresponding resistance measurements. The relative resistance change $\Delta R/R_0$ is plotted vs strain. The experiments revealed a pronounced dependency of the electrical resistivity on the mechanical load. With regard to the resistance vs strain characteristics of the MWCNT composites [Figs. 3(a) and 3(b)], it can be observed that the resistance monotonically increases with strain in the elastic regime, up to ~1.5% of mechanical strain. With further increasing strain the resistance change passes a point of inflexion and its maximum at around 4% strain. This value was found to be independent of the CNT content. At strain values of 4% and higher, the resistance monotonically decreases until final fracture of the specimen.

The carbon black nanocomposites were found to exhibit a significantly different behavior [Fig. 3(c)]. In the elastic regime, a behavior similar to the MWCNT composites is observed. However, the sensitivity, i.e., the rate of increase in resistance with strain is much higher for the CB nanocomposites [note the different scales of the resistance change axis and see Fig. 3(d) for comparison]. At strain values above the

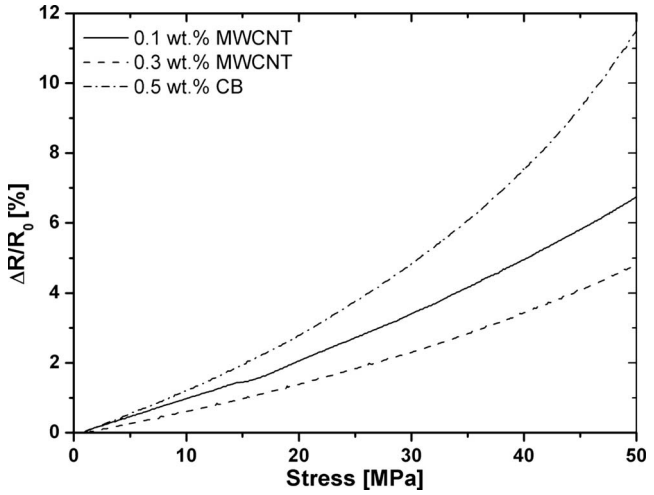

FIG. 4. Electrical resistance change vs stress in the elastic regime (50 MPa corresponds to ca. 1.5% of strain).

elastic regime, the carbon black composites exhibit a completely different behavior. Although the slope of resistance change is also decreasing at strain values higher than 2%, the curves do not go through a maximum, but pass through a point of inflexion, followed by a drastic increase in resistance shortly before final failure. In Fig. 3(d), the $\Delta R/R_0$ measurements of the three different nanocomposites are plotted into one diagram for comparative purposes.

From the results in Figs. 3(a)–3(c), it can be concluded that the piezoresistive characteristics are mainly dependent on the type of filler but also on the filler content. In the elastic regime, all nanocomposites seem to exhibit a quantitatively similar behavior. At high strain values, effects of inelastic matrix deformation will influence the conductive network and thus, particle geometry might have a stronger influence in this regime. It should be noted that the reproducibility of the resistance change vs strain measurements is very good. In the elastic regime, the piezoresistive responses of the different measurements shown in each diagram are hardly distinguishable. In the following subchapters, the elastic regime and the regime of inelastic deformation will be separately analyzed in more detail for the three nanocomposites investigated.

C. Elastic regime

Figure 4 shows the resistance change vs stress in the elastic regime. A closer look at the elastic regime clearly reveals an exponential dependence of the resistance change vs strain/stress. This behavior is in good agreement with other experimental findings and can be interpreted via an interparticle tunneling model.[16,20,47] The conduction through a network consisting of conductive particles and interparticle tunneling contacts can be approximated by a simplified analytical description of a resistor network according to Ruschau *et al.*,[48]

$$R_c = \frac{(M-1)R_t + MR_p}{N} \approx \frac{M(R_t + R_p)}{N}, \tag{1}$$

where R_c is the network (or composite) resistance, M is the number of conducting particles per path, N is the number of paths, R_t is the interparticle contact resistance and R_p is the resistance of the particles. In this approach, the conducting pathways are assumed to be connected in parallel and the resistance of pathways perpendicular to the current is neglected. If the tunneling resistance between two particles, R_t, and the resistance of the polymer matrix are much higher than the resistance of the particles, R_p, the resistance of the particles can be neglected ($R_p \approx 0$). By combining the tunneling model of Simmons[30–33] and the network approach, the composite resistance can be described as[16]

$$R_c = \frac{M}{N}\left[\frac{8\pi hs}{3d^2\gamma e^2}\exp(\gamma s)\right], \tag{2}$$

with

$$\gamma = \frac{4\pi}{h}\sqrt{2m\phi}. \tag{3}$$

Here, m and e are the electron mass and charge, d^2 is the contact area, ϕ is the height of the tunneling potential barrier, h Planck's constant and s is the thickness of the insulating film. It should be noted, that this simple model neglects any statistical distribution of the tunneling distances, as well as the real network structure and the particle geometry. In the case of high aspect ratio fillers, such as CNTs, one particle might be connected to several other neighboring particles resulting in many more possible parallel connections of pathways, than with spherical particles. In these cases, the definitions of N and M are not accurate to describe the real network structure.

In the elastic regime at low strain values the deformation of the specimen and thus the conductive network in the matrix can be assumed to be homogeneous. The relative resistance change caused by elastic deformation can then be described as

$$\frac{\Delta R}{R_0} \approx \exp[\gamma s_0(\cos^2\theta - \nu\sin^2\theta)\varepsilon] - 1, \tag{4}$$

where s_0 is the average interparticle distance in the undeformed state, ε is the applied strain and θ is the average angle between the particle contact and the direction of applied load.[49,50] θ was calculated as $\pi/4$ for rodlike particles.[47,51] Note that the values N and M do not appear in Eq. (4).

If an assumption is made for the height of the potential barrier φ, the average interparticle distance can be gained from fitting Eq. (4) to the experimental results. As pointed out in Ref. 34, the overall composite behavior can be described with single junction behavior, giving a characteristic average value for the material investigated. It should be noted that this analytical model is a simplification as it assumes mean values for interparticle distance and contact angles and also neglects any influences of contact formation or breakup. Furthermore, the strain distribution within the sample must be homogeneous. For this reason the elastic regime up to a strain value of 1% was fitted to the tunneling model. As the reproducibility of the measurements was excellent, only one exemplary measurement was fitted for the

TABLE II. Calculated values for the average interparticle distances according to the tunneling model [Eq. (4)].

Material	φ=0.2 eV	φ=0.5 eV	φ=1.0 eV
0.1 wt. % MWCNTs	2.65 nm	1.68 nm	1.19 nm
0.3 wt. % MWCNTs	1.68 nm	1.06 nm	0.75 nm
0.5 wt. % CB	3.23 nm	2.04 nm	1.45 nm

analytical analysis. In Table II the values for the average interparticle tunneling distances for s_0 are given for three assumed values of the potential barrier. Values of φ =0.1–2.5 eV are typically found in the literature for the height of the potential barrier in carbon particle/polymer matrix composites.[28,34] It can be seen that the values for the MWCNT composites do not differ significantly and are all within the same order of magnitude, confirming the arguments stated above that the particles are forming a network and are not homogeneously distributed. Thus, increasing the concentration from 0.1 to 0.3 wt. % does not lead to a significant change in interparticle distance, as it would be expected if the particles were distributed statistically. In fact, the average distance between two carbon nanotubes in a percolated path seems to be relatively constant, independent of the filler content. Comparing the values of the carbon black nanocomposite, it can be seen that the tunneling distances are significantly higher than in the case of MWCNT composites. Again, it should be noted that this analytical model is a simplification as it assumes mean values for interparticle distances and also neglects any influences of agglomerate formation and particle geometry. Therefore, the absolute values in Table II should be treated with caution. However, the method provides the possibility to quantitatively compare the different nanocomposites.

Comparing the different sensitivities of the nanocomposites resistivity vs strain, one can see from Fig. 3(d) that the carbon black containing material exhibits a more pronounced exponential behavior and the resistance increase per strain unit is significantly higher for this material. At 2% of strain, the nanocomposite containing 0.1 wt. % of MWCNTs exhibited a resistance increase of about 9%. The 0.3 wt. % MWCNT-nanocomposite showed an increase of about 6.5% in resistance at this strain value and the carbon black nanocomposite revealed a 17% resistance increase at 2% of strain. This can be explained through the aspect ratio of the particles and the resulting percolated network structure. As the carbon black nanoparticles are spherical in shape, whereas the MWCNTs may have aspect ratios of up to ~1000, the number of interparticle tunneling contacts along a conductive pathway is significantly higher in the case of CB nanocomposites. Furthermore, MWCNTs may be in electrical contact to numerous other MWCNTs along their longitudinal axis, thus resulting in a more redundant network structure. Furthermore, the orientation of the tunneling contact with respect to the direction of deformation has to be considered. The influence of contact orientation is depicted in Fig. 5. In Fig. 5, the interparticle distance s_0 between two particles is shown. Because of the applied strain ε and the lateral contraction $-\nu\varepsilon$, the interparticle distance changes with deformation. The interparticle distance s_1 after deformation can be calculated as [see Eq. (4) (Ref. 48)],

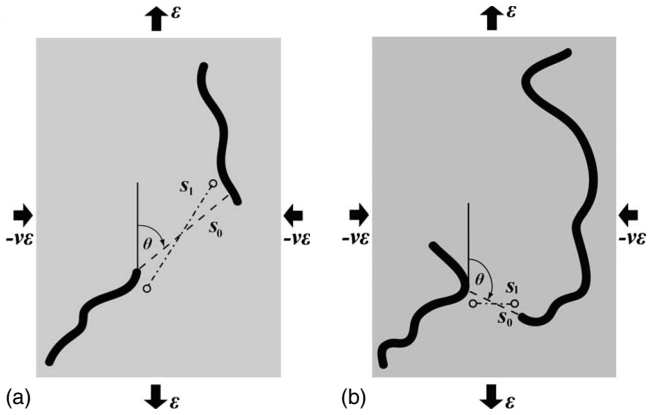

FIG. 5. (a) Influence of tensile strain on the contact distances between two CNTs, according to Ref. 48. (b) Reduced contact distance after deformation in a CNT composite. The effects of strain as well as the absolute length of the tunneling path are exaggerated for illustrational purposes.

$$s_1 = s_0[1 + \varepsilon(\cos^2\theta - \nu \sin^2\theta)]. \tag{5}$$

For spherical particles and CNTs oriented as depicted in Fig. 5(a), the interparticle distance will increase with applied tensile strain. But as the MWCNTs are randomly oriented in the bulk matrix, intertube contacts may be oriented in a manner, that even though the geometric centers of two contacting CNTs are moving apart by the applied strain, the tunneling contact distance actually decreases, as depicted in Fig. 5(b). These orientation and entanglement effects cannot occur with spherical particles. Equation (5) therefore does not deliver correct results for angles of $\theta > 90°$, which may occur in the case of high aspect ratio particles. This effect has to be considered when calculating the mean contact angles and the piezoresistive effect. The result of the contact angle effect [Fig. 5(b)] and the contact number effect is a reduced sensitivity of the electrical resistance toward strain for MWCNT composites, compared to CB composites.

It is also noteworthy, that in the case of the MWCNT nanocomposites, the resistance change vs strain in the elastic regime can be approximated reasonably well with a linear function. Up to 1.5% of strain, a linear fit can be applied to all measurements taken, with a correlation coefficient of $R^2 > 0.99$. In view of potential technical applications, this is a significant advantage, as integration into electrical measurement bridges would be facilitated for instance. The CB nanocomposites exhibit a decidedly more exponential response. In piezoresistivity theory, the slope of the curves can be interpreted as the gauge factor k,

$$\frac{\Delta R}{R} := k \cdot \varepsilon, \tag{6}$$

where

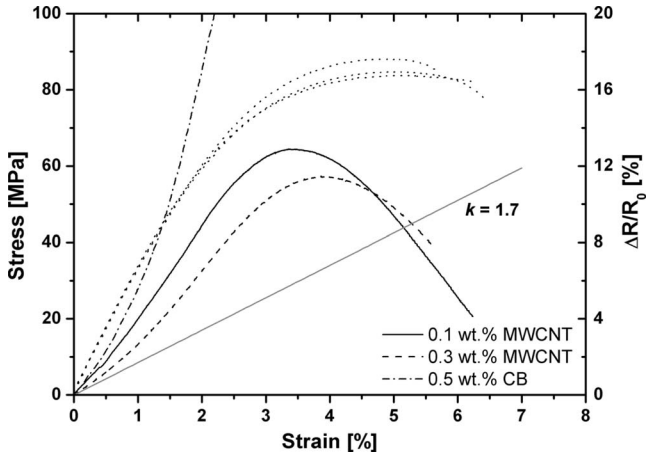

FIG. 6. Comparison of the piezoresistive response for the different nanocomposites. A linear dependency of $\Delta R/R_0$ would be expected, if the resistance change was caused by geometric deformation only [Eq. (7)]. The mechanical stress/strain curves are shown as dotted lines.

$$k := 1 + 2\nu + \frac{d\rho}{\rho \cdot d\varepsilon}. \tag{7}$$

In our experiments, k was found to range from 2.3 to 3 for 0.3 wt. % MWCNT content and from 3.4 to 4.3 for 0.1 wt. % MWCNT content. As the matrix epoxy exhibits a Poisson's ratio of 0.35, the geometric term in Eq. (7) becomes $1+2\nu=1.7$. Thus, the higher k values observed for the piezoresistive effect can be attributed to the intrinsic change in resistance, caused by the increase in the tunneling resistances (Fig. 6).

D. Plastic regime

As discussed above, at strain values higher than 2%, the tunneling fitting curves start to deviate significantly from the measured data. From Figs. 3(a)–3(c), it can be seen that the linear elastic regime of the nanocomposites ends between 1.5% and 2% of strain. At higher strain values, the resistance change vs strain curves show a strong deviation from the exponential behavior observed in the elastic regime. In the case of the MWCNT nanocomposites, the slope of resistance change decreases above the elastic regime and passes a maximum at around 4% of strain. This value was found for all measurements, independent of the MWCNT content. The CB nanocomposite exhibits a completely different behavior. The slope of resistance change is also decreasing at strain values higher than 2%, but the curves do not pass a maximum. Instead, they pass through a point of inflexion. Shortly before final failure, a drastic increase in resistance can be observed. Beyond the elastic regime, viscoelastic and inelastic deformation processes occur in the epoxy matrix, leading to irreversible changes in the percolated network of conductive particles. However, the formation of a maximum in the case of the MWCNT nanocomposites is surprising. Obviously, the pronounced differences in the resistance development at higher strain values can be attributed to the different structure of the network of conductive particles, which itself depends on several factors, such as aspect ratio, interparticle interactions etc.

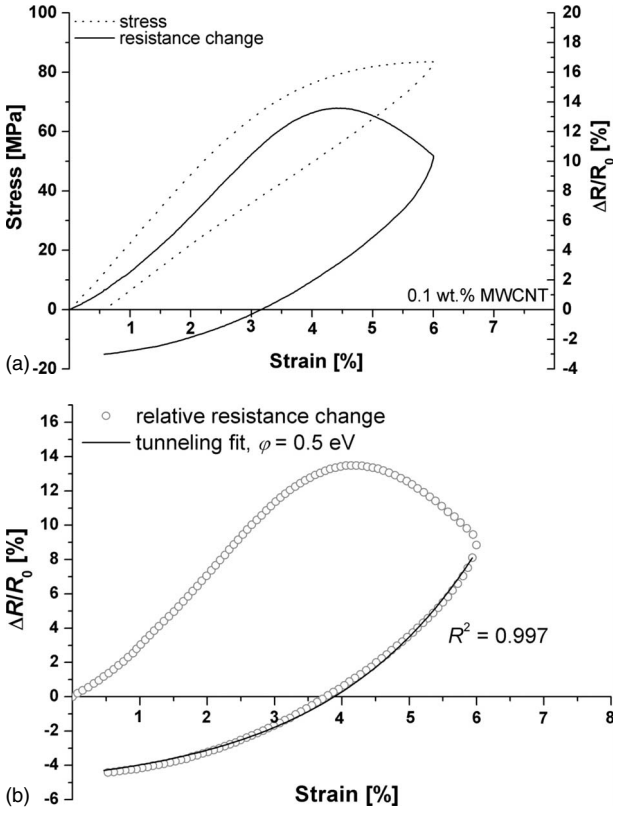

FIG. 7. (a) Stress/strain curve and corresponding piezoresistive response of the loading and unloading branch of the tensile test, (b) tunneling fit of the unloading branch according to Eq. (4).

In order to further investigate the effects occurring in the inelastic regime, modified tensile tests were performed. The specimens were subjected to a tensile strain of 6% (close to strain to failure, see Fig. 3) and subsequently unloaded to zero external stress, while the resistance was again measured simultaneously. Figure 7 shows an example of such a tensile test, performed on a 0.1 wt. % MWCNT composite. Looking at the stress-strain curve on Fig. 7(a), it can be seen that the residual strain at the end of the test is about 0.5%, i.e., the value of inelastic deformation. As the specimen was subjected to a strain value of 6%, the remaining 5.5% of strain are composed of elastic and viscoelastic deformation. Regarding the resistance change during this test, one can see from Fig. 7(a) that upon unloading the resistance decreases monotonically with strain. The maximum, occurring during loading, is not reproduced during unloading. In fact it decreases exponentially with strain, as depicted in Fig. 7(b). This suggests that the unloading process occurs by elastic resilience. A similar behavior was observed for the 0.3 wt. % MWCNT and the 0.5 wt. % CB composites.

Interestingly, all tested specimens of all nanocomposites exhibit a lower resistance after testing, even though its length increased by ~0.5%. From these results it can be concluded that the conducting network structure of nanoparticles is being irreversibly affected by viscoelastic and plastic deformation processes on the molecular level. In the case of

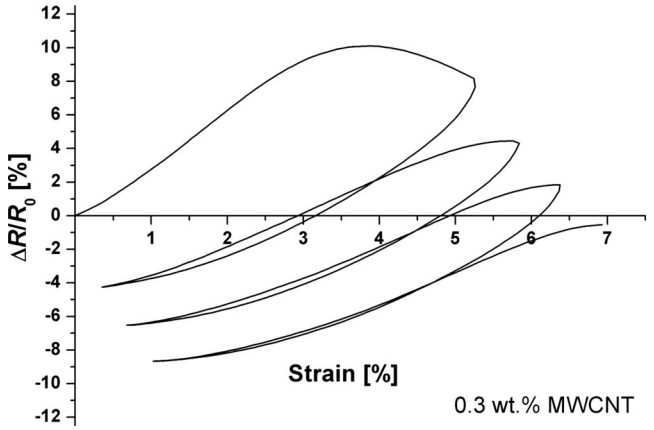

FIG. 8. Resistance change vs strain during loading and unloading of a 0.3 wt. % MWCNT composite during incremental tensile test.

MWCNTs, these effects lead to a reduction in the composite resistance above 4% of strain. In the case of spherical carbon black particles only the rate of resistance increase is reduced when the elastic regime is left, but upon unloading, it can be observed that the resistance is also irreversibly reduced. Thus, it can be concluded that the carbon black network structure is affected in a similar way by inelastic deformation as the CNT network, but the decrease in resistance is superposed by the higher sensitivity of the carbon black network vs tensile deformation, resulting in a net increase in resistance for the whole course of the tensile test. It can be assumed that orientation effects and contact formation by lateral deformation may be responsible for the reducing effect at high strain values.

In order to gain a deeper understanding of the processes leading to a decrease in resistance, a hysteresis measurement with several cycles was performed. In this incremental tensile test, the maximum strain value was chosen above 4% (5.25%) in the first cycle so that the maximum in resistance is passed and the specimen retains a permanent plastic deformation upon unloading. The maximum strain was increased in each cycle in order to achieve additional plastic deformation. The resistance change vs strain for such a test is exemplarily shown in Fig. 8. It can be observed that for each load cycle elastic resilience occurs during unloading, as discussed above (Fig. 7). Furthermore, it can be observed that the same quantitative behavior is observed for the loading section in each of the cycles. The resistance first increases exponentially with strain, but then deviates and proceeds toward a maximum. As the strain value at which the maximum occurs is shifted to higher strain values in each subsequent cycle, the maximum is only overcome in the first and second load cycle during this specific test. Thus, it can be concluded that effects of inelastic deformation are responsible for the decrease in resistance. As the onset of inelastic deformation in the epoxy is shifted to higher strain values for each cycle, the maximum of the resistance is shifted accordingly. In each cycle, additional plastic matrix deformation has a decreasing effect on the network resistance. Upon unloading, the specimens exhibited a subsequently decreasing irreversible resistance change. In the example shown in Fig. 8, the specimen exhibited a permanent resistance change of −8.5% after the third load cycle, which corresponded to an inelastic deformation of ~1%.

A further hint for the strong influence of localized inelastic deformation can be found in the resistance development of the carbon black nanocomposites at high strain values. From Fig. 3(c), it can be seen that the onset of the final drastic increase of the specimen resistance seems to be correlated with the onset of final failure. At very high strain values (around 5.5% of mechanical strain) the epoxy matrix shows the typical necking behavior in the area of the final failure. After this point is reached, the specimen deforms mostly locally and high local values of inelastic strain occur. This leads to a significant impairment of the network of spherical particles resulting in the drastic final increase in resistance, as displayed in Fig. 3(c). The resistance development of the MWCNT nanocomposites seems to be independent of an upcoming final failure, as can be seen in Figs. 3(a) and 3(b). Beyond its maximum at around 4% of strain, the resistance decreases monotonically in a nearly linear manner. A possible explanation may again be the different aspect ratio and more redundant network structure in the MWCNT composites. Instead of a rupture of the conducting pathways, the MWCNTs may be reoriented and aligned in zones of high local deformation, leading to an actual decrease in the network resistivity.

IV. CONCLUSIONS

In the present study, the potential of electrically conductive epoxy based nanocomposites for sensing stress/strain via electrical conductivity methods was investigated. The nanocomposites investigated contained 0.1 and 0.3 wt. % of MWCNTs and 0.5 wt. % of carbon black nanoparticles. It could be demonstrated that the nanocomposites produced show distinct piezoresistive behavior. The resistance vs strain response was found to exhibit a very high signal to noise ratio and high reproducibility. In the elastic regime, the piezoresistive response of the nanocomposites exhibits an exponential resistance vs strain behavior, being in agreement with the prevalent theories on charge carrier transport mechanisms in isolator/conductor composites. The macroscopic electrical conductivity, as well as the piezoresistive response of the nanocomposites is dominated by the interparticle contacts, which can be characterized by a tunneling mechanism. For the nanocomposites based on CNTs, a nearly linear dependence of resistance vs strain was observed in the elastic regime, while the CB nanocomposites exhibited a more exponential dependence. The different behavior can be explained qualitatively with the morphology of the conducting network (number of contacts, contact orientation etc), resulting from the different particle geometries. While, the MWCNT nanocomposites provide superior sensing characteristics (linearity), the CB nanocomposites reveal a higher sensitivity to mechanical deformation. At very low strain values <1%, the piezoresistive response of all nanocomposites can be approximated fairly well with a linear function.

The piezoresistive response of conductive nanocomposites may also be used to gain quantitative information about

the conducting network, i.e., the number of contacting paths, the interparticle distance etc. In this study, a simplified analytical model based on common tunneling theories was applied for a first analysis. These models need to be developed further in order to take into account parameters such as particle geometry and network formation. Because of the complexity of this topic, numerical modeling is needed to accurately reflect the structures at the nano- and microscale.[28,43,46]

ACKNOWLEDGMENTS

The financial support of the European Framework 6 Programme, Priority 4, Aeronautics and Space (Aerospace Nanotube Hybrid Composite Structures with sensing and actuating capabilities, NOESIS), Contract No. AST4-CT-2005-516150 is gratefully acknowledged.

*Corresponding author; malte.wichmann@tu-harburg.de

[1] M. Kupke, K. Schulte, and R. Schüler, Compos. Sci. Technol. **61**, 837 (2001).
[2] E. T. Thostenson and T. W. Chou, Adv. Mater. **18**, 2837 (2006).
[3] L. Böger, M. H. G. Wichmann, L. O. Meyer, and K. Schulte, Compos. Sci. Technol. **68**, 1886 (2008).
[4] J. M. Park, D. Kim, S. Kim, P. Kim, D. Yoon, and L. K. DeVries, Composites, Part B **38**, 847 (2007).
[5] E. T. Thostenson and T. W. Chou, Nanotechnology **19**, 215713 (2008).
[6] D. Bulgin, Rubber Chem. Technol. **19**, 667 (1946).
[7] P. E. Wack, R. L. Anthony, and E. Guth, J. Appl. Phys. **18**, 456 (1947).
[8] A. Voet and F. R. Cook, Rubber Chem. Technol. **41**, 1207 (1968).
[9] A. Voet, A. K. Sircar, and T. J. Mullens, Rubber Chem. Technol. **42**, 874 (1969).
[10] P. K. Pramanik, D. Khastagir, and T. N. Saha, J. Mater. Sci. **28**, 3539 (1993).
[11] J. Kost, A. Foux, and M. Narkis, Polym. Eng. Sci. **34**, 1628 (1994).
[12] F. Carmona, R. Canet, and P. Delhaes, J. Appl. Phys. **61**, 2550 (1987).
[13] X. J. Wang and D. D. L. Chung, Smart Mater. Struct. **4**, 363 (1995).
[14] V. G. Shevchenko, A. T. Ponomarenko, and C. Klason, Smart Mater. Struct. **4**, 31 (1995).
[15] A. Celzard, E. McRae, J. F. Mareche, G. Furdin, and B. Sundqvist, J. Appl. Phys. **83**, 1410 (1998).
[16] X. W. Zhang, Y. Pan, Q. Zheng, and X. S. Yi, J. Polym. Sci., Part B: Polym. Phys. **38**, 2739 (2000).
[17] L. Flandin, J. Y. Cavaille, Y. Brechet, and R. Dendievel, J. Mater. Sci. **34**, 1753 (1999).
[18] L. Flandin, Y. Brechet, and J. Y. Cavaille, Compos. Sci. Technol. **61**, 895 (2001).
[19] M. Knite, V. Teteris, B. Polyakov, and D. Erts, Mater. Sci. Eng., C **19**, 15 (2002).
[20] M. Knite, V. Teteris, A. Kiploka, and J. Kaupuzs, Sens. Actuators, A **110**, 142 (2004).
[21] I. P. Kang, K. Y. Joung, G. Choi, M. J. Schulz, Y. Choi, S. Hwang, and H. S. Ko, J. Nanosci. Nanotechnol. **7**, 3736 (2007).
[22] G. T. Pham, Y. Park, Z. Y. Liang, C. Zhang, and B. Wang, Composites, Part B **39**, 209 (2008).
[23] W. Zhang, J. Suhr, and N. A. Koratkar, J. Nanosci. Nanotechnol. **6**, 960 (2006).
[24] K. J. Loh, J. P. Lynch, B. S. Shim, and N. A. Kotov, J. Intell. Mater. Syst. Struct. **19**, 747 (2008).
[25] M. Knite, V. Tupureina, A. Fuith, J. Zavickis, and V. Teteris, Mater. Sci. Eng., C **27**, 1125 (2007).
[26] R. Zhang, M. Baxendale, and T. Peijs, Phys. Rev. B **76**, 195433 (2007).
[27] Z. Dang, M. Jiang, D. Xie, S. Yao, L. Zhang, and J. C. Bai, J. Appl. Phys. **104**, 024114 (2008).
[28] N. Hu, Y. Karube, C. Yan, Z. Masuda, and H. Fukunaga, Acta Mater. **56**, 2929 (2008).
[29] M. H. G. Wichmann, S. T. Buschhorn, L. Böger, R. Adelung, and K. Schulte, Nanotechnology **19**, 475503 (2008).
[30] J. G. Simmons, J. Appl. Phys. **34**, 1793 (1963).
[31] J. G. Simmons, J. Appl. Phys. **34**, 238 (1963).
[32] J. G. Simmons and G. J. Unterkofler, J. Appl. Phys. **34**, 1828 (1963).
[33] J. G. Simmons, J. Appl. Phys. **34**, 2581 (1963).
[34] P. Sheng, E. K. Sichel, and J. I. Gittleman, Phys. Rev. Lett. **40**, 1197 (1978).
[35] E. K. Sichel, J. I. Gittleman, and P. Sheng, Phys. Rev. B **18**, 5712 (1978).
[36] P. Sheng, Phys. Rev. B **21**, 2180 (1980).
[37] E. K. Sichel, P. Sheng, J. I. Gittleman, and S. Bozowski, Phys. Rev. B **24**, 6131 (1981).
[38] M. T. Connor, S. Roy, T. A. Ezquerra, and F. J. Balta Calleja, Phys. Rev. B **57**, 2286 (1998).
[39] J. M. Benoit, B. Corraze, and O. Chauvet, Phys. Rev. B **65**, 241405(R) (2002).
[40] F. H. Gojny, M. H. G. Wichmann, U. Koepke, B. Fiedler, and K. Schulte, Compos. Sci. Technol. **64**, 2363 (2004).
[41] F. H. Gojny, M. H. G. Wichmann, B. Fiedler, J. A. Kinloch, W. Bauhofer, A. H. Windle, and K. Schulte, Polymer **47**, 2036 (2006).
[42] W. Bauhofer and J. Z. Kovacs, Compos. Sci. Technol. **69**, 1486 (2009).
[43] C. Li, E. T. Thostenson, and T. W. Chou, Appl. Phys. Lett. **91**, 223114 (2007).
[44] C. Li, E. T. Thostenson, and T. W. Chou, Compos. Sci. Technol. **68**, 1445 (2008).
[45] N. Hu, Z. Masuda, C. Yan, G. Yamamoto, H. Fukunaga, and T. Hashida, Nanotechnology **19**, 215701 (2008).
[46] F. Dalmas, R. Dendievel, L. Chazeau, J. Y. Cavaille, and C. Gauthier, Acta Mater. **54**, 2923 (2006).
[47] M. Park, H. Kim, and J. P. Youngblood, Nanotechnology **19**, 055705 (2008).
[48] G. R. Ruschau, S. Yoshikawa, and R. E. Newnham, J. Appl. Phys. **72**, 953 (1992).
[49] T. Yasuoka, Y. Shimamura, and A. Todoroki, *Proceedings of the 9th Japan International SAMPE Symposium*, (SAMPE Japan, Tokyo, 2005), p. 341.
[50] T. Yasuoka, Y. Shimamura, and A. Todoroki, in Proceedings of the ATEM07-JSME Conference (unpublished).
[51] L. Onsager, Ann. N. Y. Acad. Sci. **51**, 627 (1949).